


New fit of timelike proton electromagnetic formfactors from e^+e^- colliders

E. Tomasi-Gustafsson ^{*}

CEA, IRFU, DPhN, Université Paris-Saclay, 91191 Gif-sur-Yvette Cedex, France

Andrea Bianconi[†]

Dipartimento di Ingegneria dell'Informazione dell'Università degli Studi di Brescia, via Branze 59, 25123 Brescia, Italy,
and Istituto Nazionale di Fisica Nucleare Sezione di Pavia, via Bassi 6, 27100 Pavia, Italy

Simone Pacetti [‡]

Dipartimento di Fisica e Geologia dell'Università degli Studi di Perugia,
and Istituto Nazionale di Fisica Nucleare Sezione di Perugia, 06123 Perugia, Italy



(Received 29 December 2020; accepted 22 February 2021; published 15 March 2021)

The data on the proton form factors in the timelike region from the BaBar, BESIII, and CMD-3 Collaborations are examined to have coherent pieces of information on the proton structure. Oscillations in the annihilation cross section, previously observed, are determined with better precision. The moduli of the individual form factors, determined for the first time, their ratios, and the angular asymmetry of the annihilation reaction $e^+e^- \rightarrow \bar{p}p$ are discussed. Fits of the available data on the cross section, the effective form factor, and the form factor ratio, allow to propose a description of the electric and magnetic timelike form factors from the threshold up to the highest momenta.

DOI: [10.1103/PhysRevC.103.035203](https://doi.org/10.1103/PhysRevC.103.035203)

I. INTRODUCTION

The understanding of the proton electromagnetic form factors (FFs), called electric $G_E(q^2)$ and magnetic $G_M(q^2)$ Sachs FFs is the aim of theoretical and experimental studies for decades, in the frame of a unified view of the scattering and annihilation regions. Much progress has been performed recently due, on one side, to new experiments that collected information with better precision and/or in a wider kinematical range and, on the other side, to theoretical efforts that extend models and parametrizations built in the space-like (SL) region to the timelike (TL) region (for a review, see Refs. [1,2]). Models based on dispersion relations [3] or vector dominance [4,5] have attempted a global description in SL and TL regions. However, not all models developed in the SL region have the correct analytical properties to be extended in the TL region where FFs are of complex nature [6].

We discuss here the data on the $e^+e^- \rightarrow \bar{p}p$ cross-section $\sigma_{e^+e^- \rightarrow \bar{p}p}$ from the BaBar, BESIII, and CMD-3 Collaborations, obtained either by direct measurements of the

annihilation process, or by means of the so-called initial state radiation (ISR) technique, i.e., by exploiting the three-body process $e^+e^- \rightarrow \bar{p}p\gamma$ where the photon is radiated by one of the initial leptons.

The emission of a real hard photon, leaving the radiating lepton in a “quasireal” state, allows extracting the cross section for the process $e^+e^- \rightarrow \bar{p}p$ from the differential cross section of the three-body process $e^+e^- \rightarrow \bar{p}p\gamma$. In such a kinematic domain, $\sigma_{e^+e^- \rightarrow \bar{p}p}$ factorizes out in the expression of the ISR differential cross section. In collinear kinematics, the ISR cross section manifests a logarithmic enhancement as a consequence of the small mass of the virtual electron that is almost on mass shell [7]. At fixed energy colliders the ISR technique allows to extract values of the $\sigma_{e^+e^- \rightarrow \bar{p}p}$ cross section at different transferred momenta, i.e., different values of q^2 (being q the four-momentum of the virtual photon in the annihilation reaction $e^+e^- \rightarrow \bar{p}p$) by tuning the kinematics of the real photon. The cost is a reduction of a factor of $\alpha = e^2/(4\pi) \simeq 1/137$ (the electromagnetic fine constant) of the number of events, that, however, can be compensated by the high luminosity recently achieved at the experimental facilities.

By means of the ISR technique and detecting the radiated hard photon, the BaBar Collaboration labeled as (BaBar) obtained data on the $e^+e^- \rightarrow \bar{p}p$ cross section with an error lower than 10% in a wide energy region from the production threshold $\sqrt{s} = 2m_p$ up to $\sqrt{s} \simeq 6$ GeV [8], where $s = q^2$ is the total energy squared in the c.m. frame of the $\bar{p}p$ system and m_p is the proton mass. Recently, using the same technique but with an undetected initial photon, the BESIII Collaboration extracted 30 values of $\sigma_{e^+e^- \rightarrow \bar{p}p}$ in the range

^{*}egle.tomasi@cea.fr

[†]andrea.bianconi@unibs.it

[‡]simone.pacetti@unipg.it

Published by the American Physical Society under the terms of the [Creative Commons Attribution 4.0 International](https://creativecommons.org/licenses/by/4.0/) license. Further distribution of this work must maintain attribution to the author(s) and the published article's title, journal citation, and DOI. Funded by SCOAP³.

of ($2 \leq \sqrt{s} \leq 3.8$) GeV [9]. The ISR photon is undetected, i.e., it is mostly emitted at small polar angles in a kinematical region uncovered by the BESIII Collaboration acceptance. This method was also used by the BaBar Collaboration where the hard condition of the photon was insured by the high energy of the colliding beams [10].

The individual determination of the moduli of the FFs in the TL region was performed by the BESIII Collaboration using the energy scan method [11] with a precision comparable to that of the data obtained in the SL scattering region. The data in the SL region were mostly collected by the JLab GEP Collaboration and published in a series of papers, summarized in Refs. [12,13]. The BESIII Collaboration has performed the individual measurement of $|G_E|$ and $|G_M|$, separately, in the TL region for the first time ever. Before such a pioneering measurement due to luminosity limitations, the information on TL FFs concerned an “effective form factor,” extracted from the total cross section and few points on a composed observable, namely, their ratio $R = |G_E|/|G_M|$, extracted from angular distribution measurements.

Let us stress that only the moduli of the FFs, which, in principle, have a nonvanishing imaginary part in the TL region, can be extracted from a precise large-statistics measurement of the angular distribution of the final-state nucleons in the e^+e^- -c.m. frame. The underlying assumption is that the reaction occurs through the one-photon exchange mechanism [14]. No measurement of the relative phase between G_E and G_M , accessible through polarization observables [15], is available yet for protons and neutrons.

Focused on the threshold region, the CMD-3 Collaboration [16] measured the cross section for the reactions $e^+e^- \rightarrow \bar{p}p\gamma$ and $e^+e^- \rightarrow \bar{n}n\gamma$. The scan of the nucleon-antinucleon threshold energy region is performed by measuring the beam energy at 0.1-MeV precision by backscattering laser light system. The energy spread due to radiation and energy resolution is low enough to differentiate the proton and neutron thresholds.

The aim of the present paper is to scrutinize the recent data on the proton FFs in the TL region, through the reaction $e^+e^- \rightarrow \bar{p}p(\gamma)$. Two characteristics, earlier predicted or highlighted, can be confirmed or infirmed by the new data: the finding of regular oscillations of the cross section [17] and the steeper q^2 dependence of the electric FF (G_E) compared to the magnetic FF (G_M) as found in the SL region [12,18]. The suggestion of a similar q^2 dependence in SL and TL regions is based on analytical properties of the amplitudes [19] and illustrated in frame of a generalized definition of FFs in Ref. [20].

In this paper we consider the new data, and we propose a global fit from threshold up to the maximum available transferred momentum. The individual TL FFs are reproduced from a fit on the ratio R and of the effective FF, allowing to extrapolate their behavior at threshold, where R is constrained to unity.

II. THE $e^+e^- \rightarrow \bar{p}p(\gamma)$ CROSS SECTION

As already pointed out, at fixed-energy e^+e^- colliders, the $e^+e^- \rightarrow \bar{p}p$ cross section, can be extracted from the data on

the differential cross section of the ISR process $e^+e^- \rightarrow \bar{p}p\gamma$, where the photon is radiated by one of the initial electrons over a range of $\bar{p}p$ energies going from the threshold $\sqrt{s_{\text{thr}}} = 2m_p$ up to the full e^+e^- -c.m. energy $\sqrt{s_{e^+e^-}}$. A similar formalism can be applied for the annihilation $e^+e^- \rightarrow \bar{n}n$.

In Ref. [8], based on the work of Ref. [21], the differential cross section for the radiative process, integrated over the nucleon momenta, was factorized into a function which depends on the photon kinematical variables multiplied by the annihilation cross section of interest for the process $e^+e^- \rightarrow \bar{p}p$,

$$\frac{d^2\sigma_{e^+e^- \rightarrow \bar{p}p\gamma}}{d\sqrt{s_{e^+e^-}} d\cos(\theta_\gamma)} = \frac{2\sqrt{s}}{s_{e^+e^-}} W(s_{e^+e^-}, E_\gamma, \theta_\gamma) \sigma_{e^+e^- \rightarrow \bar{p}p}(s),$$

$$E_\gamma = \frac{s - s_{e^+e^-}}{2\sqrt{s_{e^+e^-}}}, \quad (1)$$

where \sqrt{s} and $\sqrt{s_{e^+e^-}}$ are the invariant masses of the $\bar{p}p$ and e^+e^- systems, E_γ and θ_γ are the energy and the scattering angle of the photon in the e^+e^- -c.m. frame, whereas $W(s_{e^+e^-}, E_\gamma, \theta_\gamma)$ represents the so-called radiator function, and it gives the probability that an initial photon with energy E_γ is emitted at the angle θ_γ . In Eq. (1), the factorization of the photon variables allows to single out the elementary cross section $\sigma_{e^+e^- \rightarrow \bar{p}p}$ and extract the moduli of the TL proton FFs. However, such a factorization does fail in describing the scattering process when $\sin(\theta_\gamma) \rightarrow 0$, i.e., when the photon is radiated along the beam direction because it neglects terms depending on $(m_e^2/s_{e^+e^-})$ (m_e is the electron mass), which becomes important at small angles [7,22]. The case of final-state radiation (FSR), when the radiative emission is from the final proton or antiproton was discussed in Ref. [23]. It has been found that also the ISR-FSR interference may spoil the factorization hypothesis if the detection is not symmetric around the colliding beams axis.

The differential cross section for the annihilation process $e^+ + e^- \rightarrow \bar{p} + p$ in the Born approximation and in the c.m. frame is [14]

$$\frac{d\sigma_{e^+e^- \rightarrow \bar{p}p}}{d\Omega}(s, \theta) = \frac{\alpha^2 \beta \mathcal{C}(\beta)}{4s} \left[[1 + \cos^2(\theta)] |G_M(s)|^2 + \frac{1}{\tau} \sin^2(\theta) |G_E(s)|^2 \right], \quad (2)$$

where s is the total energy squared of the $\bar{p}p$ system $\tau = s/(4m_p^2)$ and $\beta = \sqrt{1 - 1/\tau}$ is the final particle velocity. The function,

$$\mathcal{C}(\beta) = \frac{y(\beta)}{1 - e^{-y(\beta)}}, \quad y(\beta) = \frac{\pi\alpha}{\beta} \sqrt{1 - \beta^2}$$

represents the Coulomb correction that accounts for the $\bar{p}p$ final-state interaction [24]. It becomes effective ($\gg 1$) and divergent as $\beta \rightarrow 0$. Such a divergency, that happens exactly at the production threshold, i.e., at $\beta = 0$ or equivalently at $s = 4m_p^2$, does cancel out the phase-space factor β , making finite and different from zero the cross section at the threshold.

The even $\cos \theta$ -angular dependence of the cross section of Eq. (2), in particular, the presence of the powers zero and 2 only, results directly from the Born approximation, i.e., from the assumption of one-photon exchange and the invariance of

the electromagnetic interaction with respect to parity transformation.

Following Ref. [19] in order to highlight the angular dependence, the Born differential cross section given in Eq. (2) can be written as

$$\frac{d\sigma_{e^+e^- \rightarrow \bar{p}p}}{d\Omega}(s, \theta) = \sigma_0(s)[1 + \mathcal{A}(s) \cos^2(\theta)],$$

$$\sigma_0(s) = \frac{\alpha^2 \beta \mathcal{C}(\beta)}{4s} \left(|G_M(s)|^2 + \frac{1}{\tau} |G_E(s)|^2 \right),$$

where $\sigma_0(s)$ is the differential cross section at $\theta = \pi/2$ and the function $\mathcal{A}(s)$ assuming the one-photon exchange mechanism depends on the ratio of the FFs moduli $R(s) = |G_E(s)|/|G_M(s)|$ as

$$\mathcal{A}(s) = \frac{\tau |G_M(s)|^2 - |G_E(s)|^2}{\tau |G_M(s)|^2 + |G_E(s)|^2} = \frac{\tau - R(s)^2}{\tau + R(s)^2}. \quad (3)$$

It follows that $\mathcal{A}(s)$ represents an observable which is sensitive to deviations of the differential cross section from linearity in $\cos^2(\theta)$, in particular, a residual dependence on the scattering angle θ , i.e., a non-null derivative $d\mathcal{A}/d\theta$ would mean that, besides the one-photon exchange, other intermediate states do contribute to the annihilation process $e^+e^- \leftrightarrow \bar{p}p$. Similar studies can be performed for the scattering processes $e^-p \rightarrow e^-p$ in the SL region by considering the deviation from linearity of the so-called Rosenbluth plots, see Ref. [25] and references therein.

The total cross-section $\sigma_{e^+e^- \rightarrow \bar{p}p}(s)$, obtained by integrating the differential cross section given in Eq. (2) over the solid angle $d\Omega$, namely,

$$\sigma_{e^+e^- \rightarrow \bar{p}p}(s) = \frac{4\pi \alpha^2 \beta \mathcal{C}(\beta)}{3s} \left(|G_M(s)|^2 + \frac{1}{2\tau} |G_E(s)|^2 \right) \quad (4)$$

is proportional to a s -dependent combination of the moduli squared of the FFs, which is commonly defined in terms of the effective FF $F_p(s)$, given by

$$F_p(s)^2 = \frac{2\tau |G_M(s)|^2 + |G_E(s)|^2}{2\tau + 1}. \quad (5)$$

Using such a unique effective FF is equivalent to consider the protons as a spin-zero particle and, hence, to assume $|G_E(s)| = |G_M(s)| \equiv F_p(s)$ in Eq. (2). As a consequence of their definitions in terms of the Dirac and Pauli FFs, $F_1(s)$ and $F_2(s)$,

$$G_E(s) = F_1(s) + \tau F_2(s),$$

$$G_M(s) = F_1(s) + F_2(s),$$

and the assumption of analyticity, the identity $G_E(s) = G_M(s)$ is strictly valid only at the production threshold $s = 4m_p^2$, i.e., $\tau = 1$. This phenomenon can be also interpreted as a consequence of the isotropy of the annihilation process $e^+e^- \rightarrow \bar{p}p$ just at the production threshold in the $\bar{p}p$ or e^+e^- -c.m. frame. In fact, having no preferred direction, the amplitude must be independent on the scattering angle, that implies $\mathcal{A}(4m_p^2) = 0$, see Eq. (3), i.e., $G_E(4m_p^2) = G_M(4m_p^2)$.

Therefore, a measurement of the total cross section gives access to the effective FF. The extraction of R and/or \mathcal{A}

requires in addition a precise measurement of the differential cross section. Even further precision is required for a meaningful extraction of the individual FFs. It is for this reason that it could be achieved only in the most recent experiments.

III. ANALYSIS OF THE RESULTS

A. Selected data sets

We consider four sets of data on the $\sigma_{e^+e^- \rightarrow \bar{p}p}$ cross section.

- (1) The set from the BaBar Collaboration, labeled as ‘‘BaBar,’’ has three subsets:
 - (a) Some 38 points, obtained with the ISR technique and detecting the initial photon in the range of $(1.877 \leq \sqrt{s} \leq 4.50)$ GeV, together with six points for the ratio $R = |G_E|/|G_M|$ in the range of $(1.877 \leq \sqrt{s} \leq 3)$ GeV [8].
 - (b) Some 13 points, obtained with the ISR technique and detecting the initial photon in the range of $(1.8765 \leq \sqrt{s} \leq 1.9625)$ GeV [8]. These data with a larger granularity overlap with the first four points of the above series, that, therefore, are omitted in the analysis.
 - (c) Eight points, obtained with the ISR technique and not detecting the initial photon in the range of $(3 \leq \sqrt{s} \leq 5.50)$ GeV [10].
- (2) Two sets from the BESIII Collaboration:
 - (a) Some 30 points, obtained with the ISR technique in the range of $(2.0 \leq \sqrt{s} \leq 3.60)$ GeV [9], labeled as ‘‘BESIII-ISR.’’
 - (b) Some 22 points, obtained with energy scan, together with 16 points for the ratio R and for the disentangled moduli $|G_E|$ and $|G_M|$ in the range of $(2.0 \leq \sqrt{s} \leq 3.08)$ GeV [11], labeled as ‘‘BESIII-BS.’’
- (3) A set from the CMD-3 Collaboration of 11 points, obtained with energy scan in the range of $2m_p < \sqrt{s} \leq 2.006$ GeV [16]. They belong to a subset of the published data, that includes only those points lying above the production threshold $\sqrt{s} = 2m_p$. Indeed, the complete set covers an energy interval that, as a consequence of experimental limits of the energy resolution, extends also below the physical threshold. This is the second measurement of the $\sigma_{e^+e^- \rightarrow \bar{p}p}$ cross section performed by the CMD-3 Collaboration, and it improves the first one [26] by enhancing the precision and extending the energy range. As numbers are not given in the original paper, the points (red squares in Fig. 4 of Ref. [16]) have been read from the figure. This set of data is labeled as CMD-3.

B. Confirmation of the oscillations

In Ref. [17] it was pointed out that the cross section of $e^+e^- \rightarrow \bar{p}p$ measured by the BaBar Collaboration [8] shows evidence of structures. These structures become regular when plotted as a function the three-momentum p of one of the two

TABLE I. Fit parameters from Eq. (7).

Reference	Experiments	Number	F_0	m_a^2 (GeV ²)
[8,10,17]	BaBar	85	7.7 ± 0.3	15 ± 1
[8–11]	BaBar, BESIII-ISR, and BESIII-SC	107	8.9 ± 0.2	8.8 ± 0.6

hadrons in the frame where the other one is at rest, and it is proportional to the relative velocity $\beta = \sqrt{1 - 1/\tau}$.

The BaBar Collaboration data on the modulus of the proton effective FF [8], extracted from the $e^+e^- \rightarrow \bar{p}p$ total cross section by means of the formulas given in Eqs. (4) and (5) in the range of ($2m_p < \sqrt{s} < 6$) GeV are well reproduced by the function [17],

$$F_p^{\text{fit}}(s) = F_{3p}(s) + F_{\text{osc}}[p(s)]. \quad (6)$$

It is the sum of two contributions: a dominant three-pole ($3p$) $F_{3p}(s)$, and a damped oscillatory component $F_{\text{osc}}[p(s)]$, whose expressions are

$$F_{3p}(s) = \frac{F_0}{\left(1 + \frac{s}{m_a^2}\right)\left(1 - \frac{s}{m_0^2}\right)^2}, \quad (7)$$

$$F_{\text{osc}}[p(s)] = Ae^{-Bp} \cos(Cp + D). \quad (8)$$

The explicit expressions of the variables $p = s(p)$ and $p = p(s)$ as well as of the functions in terms of s and p are explicated in the Appendix.

The $3p$ function $F_{3p}(s)$, that describes the smooth behavior (ignoring small-scale oscillations) of the effective FF, is the product of a free monopole, depending on two free parameters: the adimensional F_0 and the mass m_a , and the standard dipole with $m_0^2 = 0.71$ GeV².

The oscillatory contribution $F_{\text{osc}}[p(s)]$ reproduces the GeV-scale oscillations in the p variable. These irregularities are treated as small perturbations of the dominant smooth behavior, i.e., $|F_{\text{osc}}[p(s)]| \ll |F_{3p}(s)|$. Moreover, due to their regular periodic nature, they have a vanishing mean effect,

$$\langle F_{\text{osc}}[p(s)] \rangle_{\Delta p} \xrightarrow{\Delta p \geq 1 \text{ GeV}} 0.$$

Here we show that the recent data on F_p from the BESIII Collaboration [9,11] are compatible with those from the BaBar Collaboration [8,10] and confirm the previous findings of Ref. [17]. This is proved by the consistency of the fit parameters, obtained by including the data sets BESIII-ISR and BESIII-SC besides the BaBar one, compared to the parameters obtained by fitting the BaBar data only (Table I). In

Fig. 1(a) the cross section data are plotted as a function of p . The result of the fit using Eq. (7) is then subtracted from the data. The obtained residue \mathcal{D} [data minus $F_{3p}(s)$] displayed in Fig. 1 shows a damped and periodic oscillatory behavior, that has been fitted with the four-parameter function of Eq. (8). The values of the parameters are reported in Tables I and II together with those obtained by fitting the BaBar data only. As shown in Fig. 1, even with a slightly worse χ^2 per number of degree of freedom (n.d.f), denominated as normalized χ^2 or $\chi^2/n.d.f.$, the new fit (black solid line) follows closely the one on the only BaBar data [17] (red dashed line). Let us note that the consistency of the data obtained with different methods, beam scan, and ISR, rules out the possibility that the oscillations could be an artifact of the ISR technique or of the photon detection.

IV. GLOBAL FIT OF THE DATA

The cross section or the effective FF data can also be directly fitted with the six-parameter function $F_p^{\text{fit}}(p)$ of Eq. (6). The parameters are reported in Table III, and the fit is illustrated in Fig. 2 as a function of the relative momentum p (black solid line) together with the result from Ref. [17].

Extending the data sets does not change essentially the fit, worsening the χ^2 . The inclusion of the CMD-3 data heightens the curve in the near threshold region. The blue dashed-dot line corresponds to a constant fitted in the range of $0.1 < \sqrt{s} < 0.9$ GeV, that gives the average value of the cross section $\bar{\sigma} = 0.87 \pm 0.02$ nb. Such a value is close to the cross section at the production threshold for structureless fermions [27] as, for instance, that of the reaction $e^+e^- \rightarrow \mu^+\mu^-$. Figure 3 shows the data on the effective FF together with the curves that represent the corresponding fit functions.

A. Analysis of the formfactor ratio R

The comparison between the absolute values of the electric and magnetic FFs in the TL and SL regions can be more easily performed by considering their ratio. Exploiting the Akhiezer-Rekalo recoil proton polarization method [28,29], that represents a unique and very powerful technique to ex-

TABLE II. Fit parameters from Eq. (8) and corresponding values of the normalized χ^2 .

Reference	Data set	$A \pm \Delta A$	$B \pm \Delta B$ (GeV ⁻¹)	$C \pm \Delta C$ (GeV ⁻¹)	$D \pm \Delta D$	$\chi^2/n.d.f.$
[8,10,17]	BaBar	0.05 ± 0.01	0.59 ± 0.2	5.6 ± 0.1	0.2 ± 0.2	$57/(55-4) = 1.1$
[8–11]	BESIII-ISR, SC, and BaBar	0.07 ± 0.01	0.93 ± 0.09	5.9 ± 0.1	0.1 ± 0.2	$227/(107-4) = 2.2$

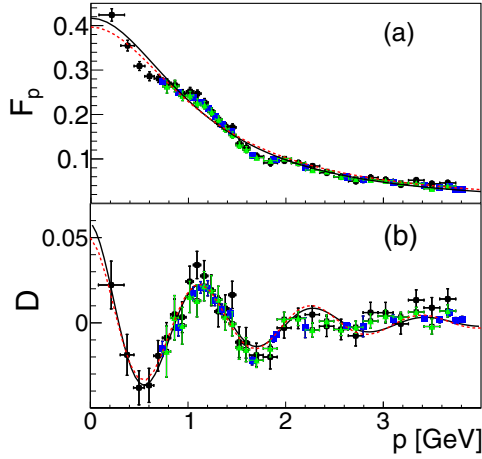


FIG. 1. (a) TL proton generalized FF as a function of p from the data of BaBar, Ref. [8] (black circles), BESIII-ISR [9] (blue squares), and BESIII-SC [11] (green triangles) with the regular background fit with Eq. (7) (black solid line); (b) data after subtraction, fitted with Eq. (8) (black solid line). For comparison the fit from Ref. [17] (red dashed lines) is also shown.

tract directly the FF ratio G_E/G_M from the longitudinal to transverse recoil proton polarization in the elastic-scattering process $\bar{e}^- p \rightarrow e^- \bar{p}$, the JLab-GEP Collaboration obtained very precise values of R in a wide region of transferred momenta [12,13]. Note that the individual FFs cannot be determined by this method. Therefore, to infer the properties of G_E , it is usually assumed that the magnetic FFs is well known from the unpolarized cross-section measurements.

In TL region, the present data from the BESIII Collaboration bring new information on the ratio of the FFs moduli with comparable precision as in the scattering region. The data from BaBar and BESIII are plotted in Fig. 4 as a function of $|q^2|$. The choice of this variable does allow to show on the same graph SL and TL values of the FF ratio and of their moduli, respectively [19].

Although the SL data (red squares in Fig. 4) show a monotone decrease, the TL ones (green triangles in Fig. 4) [11] decrease too but show the presence of oscillations not contradicting the results from the BaBar Collaboration [8] (black circles in Fig. 4). One can see a minimum in the TL range (5 to 6) GeV^2 , in correspondence with a little dip in the SL region, that should be confirmed because it lies just at the square momentum transfer corresponding to the kinematical limits of two experiments of the JLab-GEP Collaboration.

TABLE III. Six-parameter fit, Eq. (6), of the annihilation cross section $\sigma_{e^+e^- \rightarrow p\bar{p}}$ as a function of relative momentum p for the BaBar, BESIII, and CMD-3 data.

Reference	F_0	$m_a^2(\text{GeV}^2)$	A	$B(\text{GeV}^{-1})$	$C(\text{GeV}^{-1})$	D	$\chi^2/\text{n.d.f.}$
[8–11,16]	9.7 ± 0.3	7.1 ± 0.5	0.073 ± 0.007	1.05 ± 0.07	5.51 ± 0.09	0.04 ± 0.1	$278/(118-6) = 2.5$

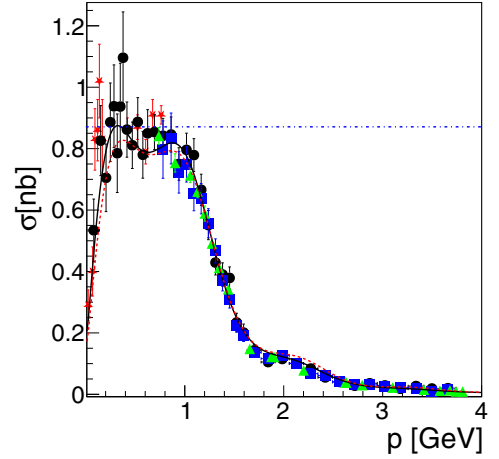


FIG. 2. Born cross section for $e^+ + e^- \rightarrow p + \bar{p}$ as a function of the momentum p . The data are from CMD-3 [16] (red stars), BaBar [8,10] (black circles), BESIII-ISR [9] (blue squares), and BESIII-SC [11] (green triangles) are shown together with the six-parameter fit from Eqs. (6)–(8) and Table III (black solid line), compared to the fit from Ref. [17] (red dashed line). The blue dashed-dot line corresponds to a constant, fitted in the range of $0.1 < \sqrt{s} < 0.9$ GeV.

The SL and TL values of the FF ratio move away with a smooth decrease from $1/\mu_p$ (μ_p is the proton magnetic moment in units of the Bohr magneton) at $q^2 = 0$ and from unity at the production threshold $q^2 = 4m_p^2$, respectively. These are the values expected from the definitions given above as well as at large transferred momenta from the QCD quark counting rules [30,31]. This is an indication that the perturbative domain has not been reached and corroborates the predictions from Ref. [20]. Following a similar approach as for the effective FF, we fit the ratio in the TL region with a function F_R reproducing a monopole decrease and a damped oscillation:

$$F_R[\omega(s)] = \frac{1}{1 + \omega^2/r_0} [1 + r_1 e^{-r_2 \omega} \sin(r_3 \omega)],$$

$$\omega = \sqrt{s} - 2m_p, \quad (9)$$

where the unitary normalization at the production threshold $F_R(4m_p^2) = 1$ is imposed. The curve representing the fit function Eq. (9), obtained with the parameters reported in Table IV is shown as a black line in Fig. 4 together with the corresponding data on the TL ratio R (black circles and green triangles). The monopole and the oscillatory components are also shown.

The red long-dashed line in Fig. 4 visualizes a one-parameter monopole function, constrained to $1/\mu_p$ at $q^2 = 0$.

TABLE IV. Four-parameter fit for R as a function of q^2 .

$r_0(\text{GeV}^2)$	r_1	$r_2(\text{GeV}^{-1})$	$r_3(\text{GeV}^{-1})$	$\chi^2/\text{n.d.f.}$
3 ± 2	0.5 ± 0.1	1.5 ± 1.2	9.3 ± 0.5	$14/(22 - 4)$

Let us recall that in the SL region the electric FF is normalized to 1 (in units of electric charge) and the magnetic FF is normalized to μ_p at $q^2 = 0$.

In Ref. [20] it was suggested that a faster decreasing behavior of the electric FF compared to the magnetic FF in the SL as well as in the TL region is expected as a consequence of the presence of an inner volume inside the nucleon that is electrically neutral (short distances corresponding to large transferred momenta). The consequence is a dipole behavior for the magnetic FF and an additional monopole decrease for the electric FF so that the ratio decreases, such as a monopole.

B. Zero crossing of the angular asymmetry \mathcal{A}

A further possibility to illustrate these results, knowing the ratio R and the fit function, is to calculate the angular asymmetry $\mathcal{A}(s)$ from Eq. (3). By definition, it assumes values in the range of $[-1, 1]$, being null at the production threshold, i.e., $\mathcal{A}(4m_p^2) = 0$. The data and the fit on \mathcal{A} are shown in Fig. 4(b).

It has been previously pointed out that, when extracted directly from the cross section, the relative error on this variable is equivalent to an error on R^2 , being, therefore, preferable for the extraction of the individual FFs [32,33].

One can see that $\mathcal{A}(s)$ crosses zero at $s = (4.62 \pm 0.07) \text{ GeV}^2$, meaning that, also at this squared momentum transferred, the modulus of the ratio is equal to one, and, hence, $|G_E| = |G_M|$. The uncertainty is obtained by varying the function in a $\pm 5\%$ range (dashed black lines). The determination of the zero crossing of \mathcal{A} gives a precise experimental constraint on FF models.

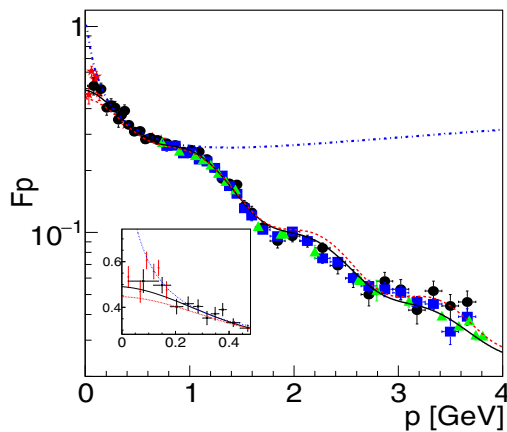


FIG. 3. Same as Fig. 2 but for the TL proton-generalized FF. The blue dashed-dot line is the expectation for a constant cross section $\sigma = 0.87 \text{ nb}$.

C. Individual formfactors $|G_E|$ and $|G_M|$

The monopole background, used to fit the FF ratio is consistent with Ref. [20] where it was suggested that the magnetic FF would follow a dipole dependence, whereas an additional monopole factor would induce a faster decrease of the electric FF in both SL and TL regions.

Overlapping the data for $|G_E|$ and $|G_M|$, extracted separately for the first time by the BESIII Collaboration [11] from $e^+e^- \rightarrow \bar{p}p$ differential cross-section data, the different behavior of the two FFs becomes visible and sizable as shown in Fig. 5. Surprisingly, $|G_E|$ and $|G_M|$ are also different at smaller q^2 , (even though they should coincide at the production threshold) and seem to converge towards small values (or to zero) at large q^2 .

One may inquire if the oscillations that are present in the cross section and in the effective FF are also visible in the individual FFs and in this case if they have to be attributed to the electric or the magnetic FF or to both of them. The modulus of the electric FF $|G_E|$ shows larger deviations from a smooth behavior, in particular, it has a dip around 5 to 6 GeV^2 , whereas $|G_M|$ follows closely a $(q^2)^{-2}$ decrease. The relations between the pairs of functions ($|G_E|$, $|G_M|$) and (R , F_p) are as follows:

$$|G_E(s)| = F_p(s) \sqrt{\frac{1 + 2\tau}{1 + 2\tau/R^2(s)}},$$

$$|G_M(s)| = F_p(s) \sqrt{\frac{1 + 2\tau}{R^2(s) + 2\tau}}. \quad (10)$$

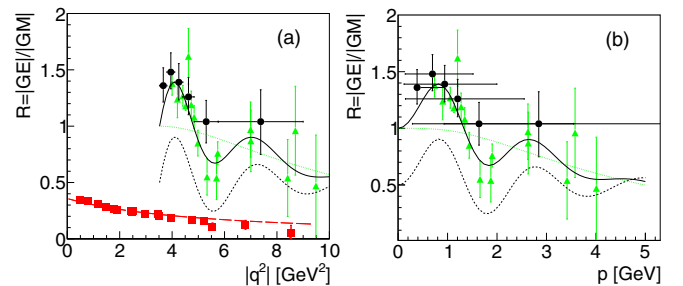


FIG. 4. Ratio $R = |G_E|/|G_M|$ as a function of (a) $|q^2|$ and (b) p from the BaBar Collaboration (black circles) [8,10] and the BES-SC Collaboration (green triangles) [11]. The solid black line is the fit from Eq. (9), decomposed in the monopole component (green dashed line) and the oscillatory component (black dotted line—shifted up by 0.5). The SL ratio from the JLab-Gep Collaboration [12] is also shown (red squares) together with its constrained monopole fit (red long-dashed line).

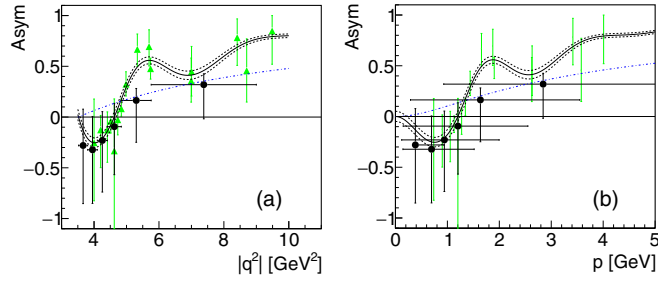


FIG. 5. Angular asymmetry as a function of $|q^2|$ (a) and of p (b) from BaBar (black circles), BESIII-SC (green triangles). The dash-dotted blue curve corresponds to a constant and unitary ratio, *i.e.*; $R = 1$, while the solid black curve is related to the fit function $F_R(s)$, with the dashed black curves representing a $\pm 5\%$ variation of the function.

By means of these expressions, the moduli of the electric and magnetic FFs can be calculated using for the ratio R and the effective FF F_p their fit function F_R , Eq. (9), and F_p^{fit} , Eq. (6), respectively. The resulting curves are shown in Fig. 5. This procedure gives, by construction, a smooth description of the individual moduli of the two FFs from the threshold up to the highest experimentally accessible values of s and represents a particular interest to illustrate the near threshold behavior as the extrapolation of the FF data is constrained by the condition $R(s = 4m_p^2) = 1$.

The result is shown in Fig. 5. Oscillations characterize both FFs, although they are smoother on $|G_M|$. By the definition of the $F_R(s)$ fit function, the convergence of the two electric and magnetic FFs, and, hence, also of the effective one, to a common value at the production threshold is implied and we find: $|G_E(4m_p^2)| = |G_M(4m_p^2)| = |F_p(4m_p^2)| \equiv F_{\text{th}} \simeq 0.48$.

Note that the QCD model fitted to the cross-section data [6] when extrapolated back to the threshold gives a com-

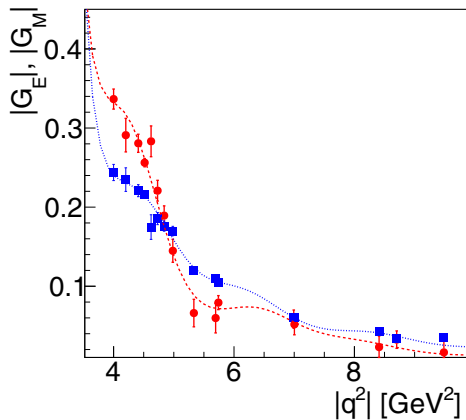


FIG. 6. $|G_E|$ (red circles) and $|G_M|$ (blue squares) from BESIII. The dashed red (dashed-dot blue) line is the calculation of $|G_E|$ and $|G_M|$ from the fits of the effective FF F_p and the ratio R .

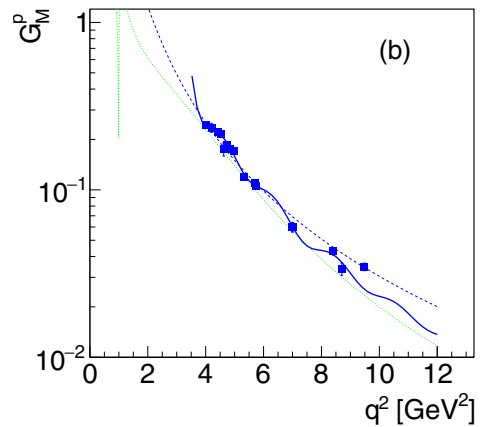
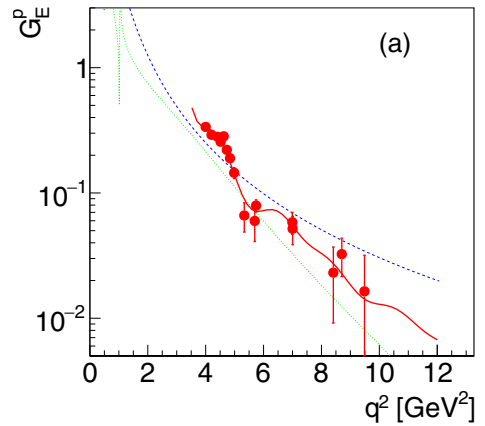


FIG. 7. (a) $|G_E|$ (red circles) and (b) $|G_M|$ (blue squares) from the BESIII Collaboration. The dashed blue (solid green) curve is the calculation of $|G_E|$ and $|G_M|$ from the QCD extrapolation [6] and from the VMD model of Ref. [2].

mon value for the FFs equal to $F_{\text{th}} \simeq 0.34$. On the other hand, the vector meson dominance (VMD) model of Ref. [2] gives $F_{\text{th}} \simeq 0.29$. The comparison between the data and these models is shown in Fig. 7. The QCD extrapolation provides, by definition, the same prediction for the two FFs as it depends on the number of the quarks involved in the process. The VMD model of Ref. [2] predicts a steeper behavior for $|G_M|$, and a number of resonances occurring in the unphysical region, *i.e.*, the portion of the TL region lying below the production threshold. Such a region is accessible through the reaction $\bar{p}p \rightarrow e^+e^-\pi^0$ [34] and can be investigated next in the future at the PANDA@FAIR facility [35].

V. DISCUSSION AND CONCLUSIONS

We have considered the recent data on TL proton FFs from Refs. [9,11,16]. These data confirm the regular oscillations found in Refs. [17,36]. We have presented a general fit of these data, that includes and updates the previous analysis. A more precise determination of the oscillation parameters has been performed. In particular, the oscillation period is a relevant parameter since it has been related to subhadron scale processes [17,36]. A similar behavior would be shown by the future $e^+e^- \rightarrow n\bar{n}$ data [37], in this case the oscillation parameters should bring information on the dynamics underlying the formation from the vacuum of quark-diquark states, the quark having a different flavor.

Our analysis does confirm a faster average decrease in the electric FF compared to the magnetic one, following a similar behavior as in the SL region. It is in agreement with the predictions of Ref. [20] where such a decreasing behavior was attributed to the existence of an electrically neutral inner region in the proton. It is also compatible with the VMD model of Ref. [2], that slightly overestimates the magnetic FF. The QCD prediction, that does not differentiate the two FFs, overestimates G_E , reproducing better G_M .

The new proton data, together with the future neutron data, will require a revision of the phenomenological models based on fitting procedures as the parameters were determined in the TL region from the effective FF only. This will be the object of a future work.

APPENDIX: EXPRESSIONS OF THE FIT FUNCTIONS

The change in variables $s = s(p)$ as well as $p = p(s)$ follows from the relations:

$$\begin{aligned} s &= 2m_p(m_p + \sqrt{p^2 + m_p^2}), \\ p &= \sqrt{s\left(\frac{s}{4m_p^2} - 1\right)}. \end{aligned} \quad (\text{A1})$$

Therefore Eqs. (7) and (8) can be rewritten as

$$\begin{aligned} F_{3p}(s) &= \frac{F_0}{\left(1 + \frac{s}{m_a^2}\right)\left(1 - \frac{s}{m_0^2}\right)^2} \\ &= \frac{F_0}{\left(1 + \frac{2m_p(m_p + \sqrt{p^2 + m_p^2})}{m_a^2}\right)\left(1 - \frac{2m_p(m_p + \sqrt{p^2 + m_p^2})}{m_0^2}\right)^2}, \end{aligned} \quad (\text{A2})$$

$$\begin{aligned} F_{\text{osc}}[p(s)] &= A \exp\left[-B\sqrt{s\left(\frac{s}{4m_p^2} - 1\right)}\right] \cos\left[C\sqrt{s\left(\frac{s}{4m_p^2} - 1\right)} + D\right] \\ &= Ae^{-Bp} \cos(Cp + D). \end{aligned} \quad (\text{A3})$$

Taking into account that $\omega = \sqrt{s} - 2m_p$, Eq. (9) can be expressed as a function of s ,

$$F_R[\omega(s)] = \frac{1}{1 + (\sqrt{s} - 2m_p)^2/r_0} \{1 + r_1 e^{-r_2(\sqrt{s} - 2m_p)} \sin[r_3(\sqrt{s} - 2m_p)]\}, \quad (\text{A4})$$

-
- [1] S. Pacetti, R. Baldini Ferroli, and E. Tomasi-Gustafsson, *Phys. Rep.* **550-551**, 1 (2015).
[2] A. Denig and G. Salme, *Prog. Part. Nucl. Phys.* **68**, 113 (2013).
[3] M. A. Belushkin, H.-W. Hammer, and U.-G. Meißner, *Phys. Rev. C* **75**, 035202 (2007).
[4] R. Bijker and F. Iachello, *Phys. Rev. C* **69**, 068201 (2004).
[5] E. L. Lomon and S. Pacetti, *Phys. Rev. D* **85**, 113004 (2012); Erratum: **86**, 039901 (2012).
[6] E. Tomasi-Gustafsson, F. Lacroix, C. Duterte, and G. Gakh, *Eur. Phys. J. A* **24**, 419 (2005).
[7] V. N. Baier, V. S. Fadin, and V. A. Khoze, *Nucl. Phys.* **B65**, 381 (1973).
[8] BaBar Collaboration, J. Lees *et al.*, *Phys. Rev. D* **87**, 092005 (2013).
[9] BESIII Collaboration, M. Ablikim *et al.*, *Phys. Rev. D* **99**, 092002 (2019).
[10] BaBar Collaboration, J. Lees *et al.*, *Phys. Rev. D* **88**, 072009 (2013).
[11] BESIII Collaboration, M. Ablikim *et al.*, *Phys. Rev. Lett.* **124**, 042001 (2020).
[12] A. J. R. Puckett *et al.*, *Phys. Rev. C* **96**, 055203 (2017); Erratum: **98**, 019907 (2018).
[13] A. J. R. Puckett *et al.*, *Phys. Rev. C* **85**, 045203 (2012).

- [14] A. Zichichi, S. Berman, N. Cabibbo, and R. Gatto, *Nuovo Cimento* **24**, 170 (1962).
- [15] A. Z. Dubničková, S. Dubnička, and M. P. Rekaló, *Nuovo Cimento Soc. Ital. Fis., A* **109**, 241 (1996).
- [16] CMD-3 Collaboration, R. R. Akhmetshin *et al.*, *Phys. Lett. B* **794**, 64 (2019).
- [17] A. Bianconi and E. Tomasi-Gustafsson, *Phys. Rev. Lett.* **114**, 232301 (2015).
- [18] The Jefferson Lab Hall A Collaboration, M. Jones *et al.*, *Phys. Rev. Lett.* **84**, 1398 (2000).
- [19] E. Tomasi-Gustafsson and M. P. Rekaló, *Phys. Lett. B* **504**, 291 (2001).
- [20] E. Kuraev, E. Tomasi-Gustafsson, and A. Dbeyssi, *Phys. Lett. B* **712**, 240 (2012).
- [21] G. Bonneau and F. Martin, *Nucl. Phys.* **B27**, 381 (1971).
- [22] M. Benayoun, S. I. Eidelman, V. N. Ivanchenko, and Z. K. Silagadze, *Mod. Phys. Lett. A* **14**, 2605 (1999).
- [23] V. V. Bytev, E. A. Kuraev, E. Tomasi-Gustafsson, and S. Pacetti, *Phys. Rev. D* **84**, 017301 (2011).
- [24] A. H. Hoang, in *Proceedings, 31st Rencontres de Moriond, Leptonic Session, Les Arcs, France, March 16-23, 1996*, edited by J. Trân Thanh Vân (Frontieres, France, 1996), pp. 129–134.
- [25] G. Gakh and E. Tomasi-Gustafsson, *Nucl. Phys.* **A761**, 120 (2005).
- [26] CMD-3 Collaboration, R. R. Akhmetshin *et al.*, *Phys. Lett. B* **759**, 634 (2016).
- [27] R. Baldini, S. Pacetti, A. Zallo, and A. Zichichi, *Eur. Phys. J. A* **39**, 315 (2009).
- [28] A. Akhiezer and M. P. Rekaló, *Dokl. Akad. Nauk. Ser.Fiz.* **180**, 1081 (1968) [*Sov. Phys. Dokl.* **13**, 572 (1968)].
- [29] A. I. Akhiezer and M. P. Rekaló, *Fiz. Elem. Chast. Atom. Yadra* **4**, 662 (1973) [*Sov. J. Part. Nucl.* **4**, 277 (1974)].
- [30] V. Matveev, R. Muradyan, and A. Tavkhelidze, *Teor. Mat. Fiz.* **15**, 332 (1973).
- [31] S. J. Brodsky and G. R. Farrar, *Phys. Rev. Lett.* **31**, 1153 (1973).
- [32] PANDA Collaboration, B. Singh *et al.*, *Eur. Phys. J. A* **52**, 325 (2016).
- [33] PANDA Collaboration, E. Tomasi-Gustafsson and A. Dbeyssi, *EPJ Web Conf.* **66**, 06024 (2014)EWCPBI.
- [34] C. Adamušćín, E. A. Kuraev, E. Tomasi-Gustafsson, and F. E. Maas, *Phys. Rev. C* **75**, 045205 (2007).
- [35] PANDA Collaboration, J. Ritman, *Int. J. Mod. Phys. A* **20**, 567 (2005).
- [36] A. Bianconi and E. Tomasi-Gustafsson, *Phys. Rev. C* **95**, 015204 (2017).
- [37] BESIII Collaboration, S. Ahmed, in *3th European Research Conference on Electromagnetic Interactions with Nucleons and Nuclei, Paphos, Cyprus, 2019* (EINN, Paphos, Greece, 2020).